



Tunable Assembly of Biomimetic Peptoids as Templates to Control Nanostructure Catalytic Activity

Journal:	<i>Nanoscale</i>
Manuscript ID	NR-ART-05-2018-003852.R1
Article Type:	Paper
Date Submitted by the Author:	08-Jun-2018
Complete List of Authors:	Merrill, Nicholas; University of Miami, Dept of Chemistry Yan, Feng; Pacific Northwest National Laboratory, Physical Sciences Division Jin, Haibao; Pacific Northwest National Laboratory, Physical Sciences Division Mu, Peng; Pacific Northwest National Laboratory, Physical Sciences Division Chen, Chun-Long; Pacific Northwest National Laboratory, Physical Sciences Division Knecht, Marc; University of Miami, Department of Chemistry



Journal Name

ARTICLE

Tunable Assembly of Biomimetic Peptoids as Templates to Control Nanostructure Catalytic Activity

Nicholas A. Merrill,^{†,a} Feng Yan,^{†,b,c} Haibao Jin,^b Peng Mu,^{b,d} Chun-Long Chen,^{b,*} and Marc R. Knecht^{a,3,*}

Received 00th January 20xx,
Accepted 00th January 20xx

DOI: 10.1039/x0xx00000x

www.rsc.org/

Nanostructured materials present new opportunities to achieve sustainable catalytic reactivity. Fabrication and organization of these catalytic particles for enhanced reactivity remain challenging due to limited synthetic and organization strategies. Biomimetic approaches represent new avenues to address such challenges. Here we report the tunable assembly of sequence-defined peptoids as templates to control the formation of highly reactive Pd nanostructures of different arrangements. In this regard, peptoid 2D membranes and 1D fibers were assembled and used to template Pd nanoparticles in specific orientations. Catalytic analysis of the resulting materials demonstrated enhanced reactivity from the fiber-based system due to changes in inorganic material display. These results suggest that the morphology of peptoid-based templates plays an important role in controlling material properties, which could open a new direction of using the peptoid assembly for applications in optics, plasmonics, sensing, etc.

Introduction

The three dimensional (3D) arrangement of nanoparticle (NP) catalysts offers enhanced capabilities for tandem and selective reactions; however, approaches to achieve these structures remain limited.¹⁻³ Current methods include manipulating NP-NP interactions for assembly⁴⁻⁶ and elegant site-selective NP growth and organization strategies to orient NPs for optimal activity.⁷⁻⁹ Conversely, biology exploits exquisite control over the synthesis, arrangement, and application of a diverse set of nanostructures.^{2, 3, 10-14} Unfortunately, the translation of bio-based approaches to catalysis is complicated by the intricate folding of biomolecules and their destabilization under typical reaction conditions where elevated temperatures or organic solvents are frequently used. To overcome these limitations, biomimetic systems that provide the capabilities accessed by biology while remaining stable under different conditions are necessary.

Peptoids, poly-*N*-substituted glycines, were recently developed to mimic proteins and peptides and bridge the gap with traditional polymers.¹⁵ Peptoids can be synthesized with greater side chain diversity than peptides, and they are

protease resistant, as well as chemically and thermally stable. Moreover, peptoids offer unique opportunities for controllable self-assembly of hierarchical structures¹⁶⁻²³ and for biomimetic crystallization²⁴⁻²⁷ as their lack of backbone hydrogen bonds simplifies inter-peptoid and peptoid-surface interactions exclusively through side chain chemistries. All of these features make sequence-defined peptoids ideal biomimetic templates to control the formation and organization of catalytic NPs with tailored properties.

Recently, we demonstrated the assembly of peptoid Pep_{Pd}-1 into highly stable and crystalline 2D nanomembranes.¹⁸ The resultant membranes have lipid bilayer like thicknesses, responsiveness to changes in ionic strength, and the ability to self-repair. Moreover, they are superior to lipid bilayers and other 2D materials because: 1) they are free-standing, highly stable, and atomically ordered, and 2) attaching a broad range of functional groups at various locations in the peptoid sequence leaves this basic membrane structure intact. Pep_{Pd}-1 has two sub-blocks that contain, respectively, six polar monomers, *N*-(2-carboxyethyl)glycine (Nce), and six nonpolar monomers, *N*-[2-(4-chlorophenyl)ethyl]glycines (N_{4-CI}pe); the *N*-terminus was conjugated with one 6-aminohexanoic acid (Aha). Because both the amine and carboxylate groups of Pep_{Pd}-1 are known to bind Pd,²⁸ herein, we demonstrate the ability to tune the morphology of Pep_{Pd}-1 assembly and exploit this tunable assembly to template the formation of highly catalytic Pd nanomaterials (Scheme 1).

In this contribution, the generation of Pd nanomaterials templated by peptoid assemblies with two different morphologies is processed. Via changes in the underlying template morphology, differences in both the inorganic material assembly and resultant catalytic activity were evident.

^a Department of Chemistry, University of Miami, 1301 Memorial Drive, Coral Gables, Florida 33146, USA. E-mail: knecht@miami.edu

^b Physical Sciences Division, Pacific Northwest National Laboratory, Richland, Washington 99352, USA. E-mail: Chunlong.Chen@pnl.gov

^c College of Chemistry & Chemical Engineering, Linyi University, Linyi, Shandong 276005, China.

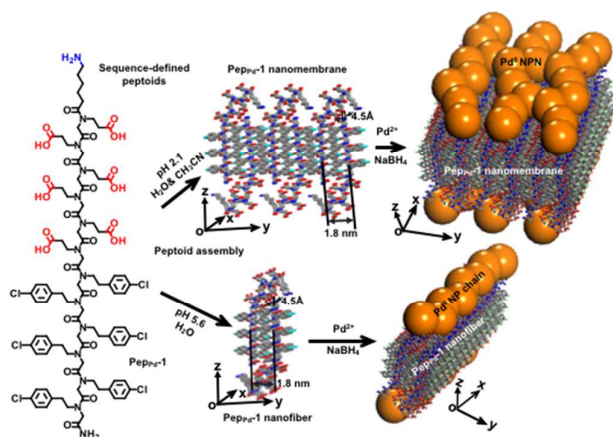
^d Department of Mechanical Engineering and Materials Science and Engineering Program, State University of New York, Binghamton, NY 13902, USA.

[†]These authors contributed equally.

Electronic Supplementary Information (ESI) available: [synthetic methods and additional TEM analysis]. See DOI: 10.1039/x0xx00000x

The materials were initially characterized using standard spectroscopic and microscopic methods to confirm Pd material production, after which they were used to drive olefin hydrogenation, an industrially important reaction. Our results show that the catalytic activity of the peptoid templated Pd nanomaterials is dependent on the morphology of underlying peptoid assembly, in which those templated by fiber-like $\text{Pep}_{\text{Pd-1}}$ assemblies exhibited significant enhancement for olefin hydrogenation over the materials templated by the $\text{Pep}_{\text{Pd-1}}$ 2D membranes. It is anticipated that this effect arises from the inorganic material display that optimizes the structures for interactions with reagents in solution, which, in turn, enhances the catalytic reactivity.

Scheme 1. Pd⁰ NP fabrication and morphology control via peptoid templates of selectable morphologies.



Materials and Methods

Materials. β -alanine *t*-butyl ester hydrochloride was purchased from Chem-Impex International, Inc. The hydrochloride was deprotected by a sodium hydroxide aqueous solution and then extracted with CH_2Cl_2 , filtered, and rotary evaporated for further use. All other amine submonomers and other reagents were obtained from commercial sources and used without further purification. K_2PdCl_4 , allyl alcohol, 3-buten-2-ol, and antifoam SE-15 were purchased from Sigma-Aldrich. NaBH_4 was acquired from Acros Organics. Finally, MilliQ water at $18 \text{ M}\Omega\cdot\text{cm}$ was used for all water-based experiments.

Synthesis of amphiphilic peptoid. $\text{Pep}_{\text{Pd-1}}$ was synthesized by using a modified solid-phase submonomer synthesis method as described previously.^{26, 29} The rink amide resin (0.09 mmol) was treated with a DMF solution of Fmoc-6-aminohexanoic acid (1.5 mL, 0.09 mmol) and 0.50 mL of 50% (v/v) *N,N*-diisopropylcarbodiimide (DIC)/DMF. The mixture was agitated overnight at room temperature, filtered, and washed with DMF. For all DMF washes, 1 mL DMF was added and then agitated for 1 min (repeated five times). In the next step, the terminal Fmoc groups were deprotected by adding 2 mL of 20% (v/v) 4-methylpiperidine/DMF. The mixture was agitated

for 40 min, filtered, and washed with DMF. The final crude product was cleaved from the resin by addition of 95% trifluoroacetic acid (TFA) in water, which was then evaporated off under a stream of N_2 gas. Finally, crude peptoids were dissolved in $\text{H}_2\text{O}/\text{CH}_3\text{CN}$ (v/v=1:1) for HPLC purification. Purified peptoids were analyzed using a Waters ACQUITY reverse-phase UPLC (55 - 75% gradient at 0.4 mL/min over 7 min at 40°C with a ACQUITY[®]BEH C18, 1.7 μm , 2.1 mm \times 50 mm column) that was connected with a Waters SQD2 mass spectrometry system. The final peptoid product was lyophilized at least twice from its solution in a mixture (v/v = 1:1) of water and acetonitrile. The peptoid powder was finally divided into small portions (2.0×10^{-6} mol) and stored at -80°C .

Peptoid self-assembly. To generate peptoid membranes, the lyophilized $\text{Pep}_{\text{Pd-1}}$ (2 μmol , 4.16 mg) was dissolved in 400 μL of $\text{H}_2\text{O}/\text{CH}_3\text{CN}$ (pH=2.1) via agitation to complete dissolution. Slow evaporation at 4°C over 2 days was used where gel-like materials containing large amounts of peptoid membranes were obtained. For the production of the peptoid fibers, lyophilized $\text{Pep}_{\text{Pd-1}}$ (2 μmol , 4.16 mg) was first mixed with 1.0 mL of deionized water, to which a few drops of 2.0 M aqueous solution of NaOH were then added to bring a final solution pH to 5.6 to obtain the aqueous solution with a large amount of $\text{Pep}_{\text{Pd-1}}$ nanofibers (Confirmed by TEM and AFM images shown in below).

Characterization of Peptoid Membranes and Fibers. TEM was performed on an FEI Tecnai instrument operating at an accelerating voltage of 200 kV. For TEM measurement, a 2 μL drop of the assembly solution was diluted in 5 μL of deionized water and put onto a carbon-coated Cu grid for 10 min. For negative staining, after the droplet was dried by filter paper, 5 μL of phosphotungstic acid (wt 2%) was then dropped onto the TEM grid for 2 min. Finally the droplet was dried by filter paper, and the resulting TEM grid was used for TEM imaging.

AFM tests were performed on a Bruker MultiMode 8 by using tapping mode or ScanAsyst mode at room temperature. For AFM measurements, a 2 μL drop of the assembly solution was diluted with deionized water and placed onto a freshly cleaved mica substrate for 2 min. The solution was dried by filter paper.

Synthesis of Peptoid Assembly Templated Pd Nanomaterials. Pd nanomaterials were synthesized at a 50, 60, 70, and 80:1 metal:peptoid assembly (membranes or fibers) ratio. In this regard, 4.93 μL of a 10 mg/mL peptoid assembly stock solution was added to 3.00 mL of water. To this solution, 11.9, 14.2, 16.6, or 19.0 μL of 0.1 M K_2PdCl_4 in water was added to obtain the 50, 60, 70, or 80:1 metal : peptoid assembly ratio, respectively. The solutions were then mixed and the metal ions were allowed to incubate with the peptoid templates for 15.0 min. Next, 59.3, 71.1, 83.0, or 94.9 μL of NaBH_4 was added to each system, respectively, to reduce the Pd^{2+} ions to Pd^0 . The materials were then allowed to reduce for 1 h at room temperature.

Characterization of Pd⁰ Nanoparticles Templated by Peptoid Assembly. UV-vis spectra were obtained using an Agilent 8453 spectrometer using a 2.0 mm quartz cuvette cleaned with aqua regia. A Phillips CM200 TEM operating at

200 kV was used for lower resolution TEM analysis where samples were made by dropcasting 5 μL of the materials onto a 200 mesh carbon-coated TEM grid (Ted Pella). HR-TEM was conducted on an FEI Tecnai or JEM 2100 (JEOL) instrument operating at an accelerating voltage of 200 kV. Nanoparticle size was determined using Image J.

Hydrogenation of Olefins. To determine the catalytic reactivity of Pd nanomaterials templated by peptoid assembly, the hydrogenation of allyl alcohol and 3-buten-2-ol was conducted with minor changes from previous studies.³⁰⁻³² To maintain a 0.05 mol% Pd loading, the nanoparticle and water volumes were varied for each metal:peptoid assembly ratio in a 50.0 mL reaction volume. For example, using the 50:1 materials, 1.59 mL of templated nanoparticles were added to 23.41 mL of water in a 250 mL three-neck round bottom flask, along with 20.0 μL of antifoam SE-15. To saturate the Pd surface with hydrogen, H_2 gas was bubbled into the solution for 30 min at a gauge pressure of 50 kPa. The hydrogenation reaction was then initiated by the addition of a 50.0 mM olefin solution resulting in a 25.0 mM reaction concentration. Aliquots were then removed at 0, 1, 5, 10, 15, 20, 30, 40, 50, and 60 min and analyzed using an Agilent 7820A GC equipped with a DB-ALC1 column and a flame ionization detector.

Results and Discussion

Free-standing 2D membranes were assembled from $\text{Pep}_{\text{Pd-1}}$ at pH 2.1 in a $\text{H}_2\text{O}/\text{CH}_3\text{CN}$ solvent, while 1D fibers from the same peptoid were generated in water only at a pH of 5.6. AFM and TEM analysis of the final assembled materials confirmed these morphologies (Figures 1a and b, and Electronic Supplementary Information (ESI), Figure S1). Analysis of the peptoid assemblies indicated that the membranes were ~ 3.5 nm thick, as determined from the AFM height results, while the fiber structures were 4.7 ± 0.7 nm in diameter according to statistical TEM analysis (ESI, Figure S2). Additional X-ray diffraction (XRD) studies of the peptoid assemblies demonstrated that the membranes assembled from $\text{Pep}_{\text{Pd-1}}$ were highly crystalline (Figure 1c). The strongest peak at 4.5 \AA corresponds to the alignment of peptoid backbone chains along the x-direction, while the 1.8 nm spacing corresponds to the distance between two peptoid backbones packed inside the membranes with N4-CIpe groups facing each other (Scheme 1).¹⁸ In contrast to the membranes, the fibers assembled from $\text{Pep}_{\text{Pd-1}}$ were less crystalline with the loss of many peaks that were observed for membranes (Figure 1c). Interestingly, the observation of peaks at 4.5 \AA and 1.8 nm indicated that similar inter-backbone distances were found for fibers along the x- and y-directions, as compared to the membranes (Scheme 1).

Based upon the microscopic imaging and XRD analysis of the materials, important information concerning their molecular level conformation can be accessed. We reasoned that when the solution pH was changed from 2.1 (for membrane formation) to 5.6 (for fiber generation), the hydrophilic block of $\text{Pep}_{\text{Pd-1}}$ became partially ionic (ESI, Figure S3), resulting in increased electrostatic repulsion that drives

nanofiber formation. This increase in ionic repulsion of the hydrophilic groups of the nanofibers makes the packing of the hydrophobic groups less ordered as compared to the same region within the membranes; this explains the lower crystallinity of nanofibers in contrast to membranes (Figure 1c). On the other hand, the increased electrostatic repulsion between the hydrophilic blocks of $\text{Pep}_{\text{Pd-1}}$ makes them sufficient to cover the hydrophobic domains of $\text{Pep}_{\text{Pd-1}}$ in the fiber packing (Scheme 1, and ESI, Figure S4). The hydrophilic blocks of $\text{Pep}_{\text{Pd-1}}$ in both the membranes and fibers are exposed to an aqueous environment, and such exposure is important for these assemblies to act as biomimetic templates for complexation of metal ions. Once bound, these ions can be reduced to generate the zerovalent metal NPs at the peptoid surface, which are stabilized by the template to prevent material aggregation in solution to bulk structures.

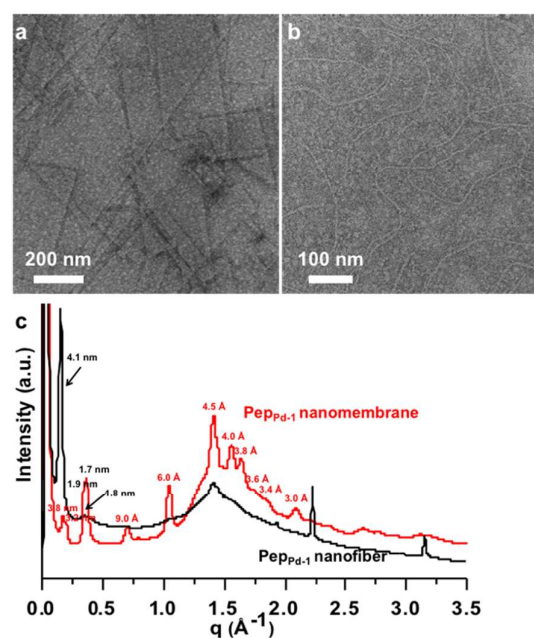


Figure 1. Characterization of peptoid assemblies. (a) Negatively stained TEM image showing the assembled $\text{Pep}_{\text{Pd-1}}$ membranes. (b) Negatively stained TEM image showing the assembled $\text{Pep}_{\text{Pd-1}}$ fibers. (c) XRD of the $\text{Pep}_{\text{Pd-1}}$ membrane (red) and fiber (black).

Based upon the morphology of the underlying peptoid assembly templates, changes in the metallic morphology of inorganic catalytic nanomaterials grown on their surfaces were anticipated that could impact their reactivity performance. To generate the metallic Pd materials, Pd^{2+} ions were first mixed with pre-assembled $\text{Pep}_{\text{Pd-1}}$ membranes or fibers dispersed in water. After complex formation, NaBH_4 was then used to reduce the metal ions and initiate Pd NP formation. To examine the effect of Pd^{2+} loading on the morphology of the resulting Pd nanomaterials on the peptoid templates, the Pd^{2+} concentration was varied over a Pd^{2+} :peptoid ratio of 50 - 80. To differentiate between the materials, the samples are

referred to as M/F-PdX, where M (membrane) or F (fiber) describes the underlying template morphology, while X represents the Pd²⁺:peptoid assembly ratio employed during nanoparticle synthesis.

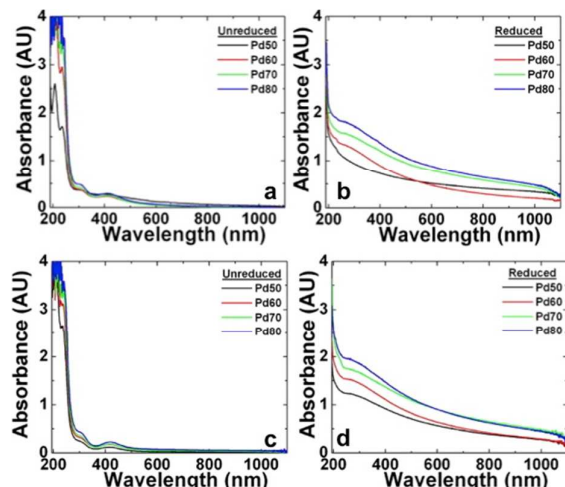


Figure 2. UV-vis analysis of Pd materials fabricated using the membrane template (a) before and (b) after reduction. Analysis of the Pd materials fabricated using the fiber template (c) before and (d) after reduction.

The formation of Pd NPs was initially monitored using UV-vis spectroscopy (Figure 2). In general, the 236 nm absorbance of the Pd²⁺ ions in the presence of the peptoid templates disappeared upon reduction. This effect was also observed concurrent with an increase in absorbance towards lower wavelengths for the reduced materials, consistent with NP formation.³³ The absorbance intensity of the Pd containing materials was proportional to the metal ion concentration where no absorbance differences based upon template morphology were noted. To this end, the spectra of the materials templated by the peptoid fibers or membranes were nearly identical when using the same Pd²⁺:peptoid ratio for NP production.

The final composite materials were next characterized using TEM to identify the morphology of the Pd component. When the membranes were used as the template, the obtained Pd materials were networks of interconnected nanoparticles, termed nanoparticle networks (NPNs - Figure 3 and ESI, Figure S5). The M-Pd50 sample produced Pd NPNs that were polycrystalline with an average width of 5.1 ± 0.9 nm (Figure 3a and ESI Figure S6a). Upon increasing the metal loading in the M-Pd60 sample, Pd NPNs were again generated with an average width of 5.6 ± 1.1 nm (Figure 3b and ESI Figure S6b). At the two highest metal loadings using the membrane template, M-Pd70 and M-Pd80, the Pd NPNs appeared to become denser. In these samples, their average widths were 5.3 ± 1.1 nm (Figure 3c and ESI Figure S6c) and 5.7 ± 1.2 nm (Figure 3d and ESI Figure S6d), respectively. High-resolution TEM (HR-TEM - Figure 3 inserts and ESI, Figure S5) demonstrated that the materials were polycrystalline, likely arising from the aggregation of individual NPs to generate the NPN structure (Scheme 1).

TEM analysis showed that the Pd nanomaterials templated by the Pep_{Pd}-1 fibers generally exhibited different morphologies, as compared to the materials prepared by the membranes. For the fiber-templated structures, Pd⁰ NP chains

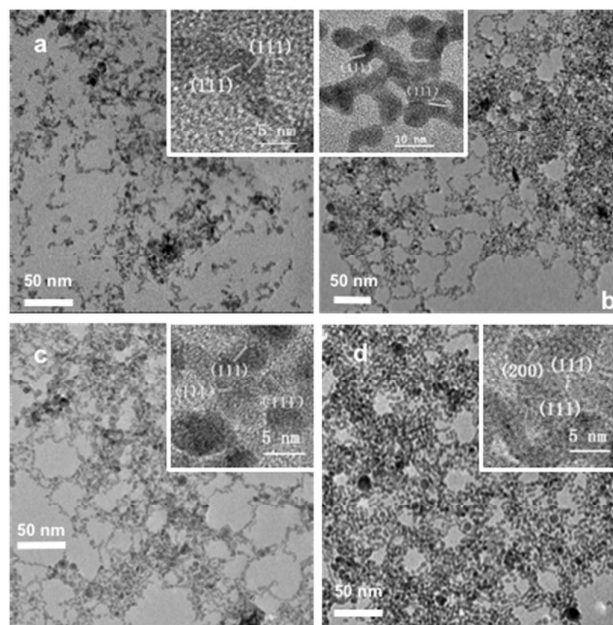


Figure 3. TEM images of Pd nanomaterials templated by the peptoid-membrane: (a) M-Pd50, (b) M-Pd60, (c) M-Pd70, and (d) M-Pd80. Inserts are HR-TEM images of each sample.

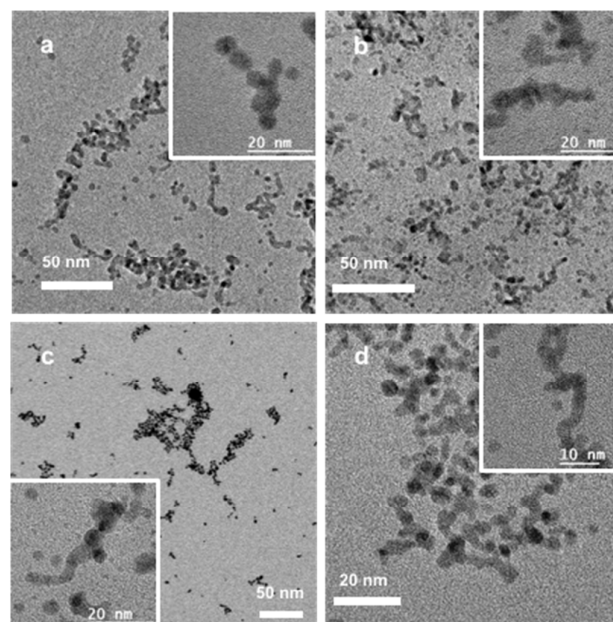


Figure 4. TEM images of Pd nanomaterials templated by the peptoid-fiber: (a) F-Pd50, (b) F-Pd60, (c) F-Pd70, and (d) F-Pd80. Inserts are HR-TEM images for each sample.

appeared to be the predominate structure (Figure 4, and ESI, Figures S7 and S8). Specifically, in the F-Pd50 sample, Pd⁰ NP chains with an average width of 5.4 ± 0.8 nm were observed (Figure 4a and ESI, Figures S7a and S8a). Similar Pd⁰ NP chains

were observed for the F-Pd60, F-Pd70, and F-Pd80 materials. For these samples, the average chain width remained narrow with values of 5.4 ± 1.0 nm, 5.2 ± 1.3 nm, and 5.0 ± 0.9 nm, respectively. HR-TEM (Figure 4 insert and ESI, Figure S7) indicated that the structures were polycrystalline, as anticipated.

Taken together, these results suggest that the morphologies of the starting peptoid assembly templates play a role in the final morphology of resulting Pd⁰ nanomaterials. Although the exact mechanism of Pd⁰ nanostructure formation remains unclear, based upon the morphologies of the peptoid templates, it is anticipated that the Pd materials are bound to the surface of the template. This would sequester the biomimetic component inside the composite structure to form the final material. As shown previously,³⁴ when Pd²⁺ ions are reduced in the absence of a stabilizing template under the conditions employed here, bulk Pd precipitation was observed. To characterize the structural morphology of the peptoid-based materials, negative stained TEM analysis was conducted. The negative stain was required due to the low Z composition of the template that leads to its inability to be observed via conventional TEM methods. For this, the peptoid-templated Pd⁰-coated structures were deposited onto a TEM grid, followed by staining with 2% phosphotungstic acid. TEM imaging of the materials was then processed, where no observation of the peptoid template was noted.

Additional control studies to monitor structural changes of the peptoid assembly template during material synthesis were conducted. In this regard, the peptoid membranes (0.24 M) and fibers (0.048 M) were incubated with 1.2 mM Na₂PdCl₄ for 15 min. The samples were then imaged via AFM (ESI, Figure S9). From these images, the templates clearly were present in the sample where deposits of the secondary material on the peptoid surface were evident. As such, it is possible that the reduction process employing NaBH₄ may lead to peptoid structural changes, resulting in the observed final composite materials. It is also possible that small Pd NPs were able to enter into the inner core of template, which could disrupt the 3D structure as reported previously.³⁵ Nevertheless, it appears that the templates play a critical role in the formation and stabilization of Pd nanomaterials.

Overall, the Pd⁰ nanomaterial morphology generally appeared to be dependent upon the metal loading and the underlying peptoid assembly template morphology. It was observed that the M-Pd samples resulted in Pd NPN structures, while the F-Pd samples tended to produce metallic materials that reflected chains of interconnected nanoparticles. In both templates, the Pd²⁺ ions are anticipated to bind at the carboxyl, amine, and amide groups exposed at the surface of the biomimetic scaffolds.^{31, 34} Our AFM analysis of the peptoid assembly templates in the presence of Pd²⁺ confirmed material deposition (ESI, Figure S9). Upon reduction, Pd⁰ NPs rapidly form. For the membrane-based structures, the NPs are dispersed on a flat surface. As the Pd loading increases, the interparticle distance decreases, leading to NP aggregation to form the NPNs. For the fiber template, Pd again nucleated on the surface of peptoid assembly. With

increasing amounts of metal in the sample, the Pd NPs are anticipated to aggregate over the curved surface. The curvature of the fiber, as compared to the flat surface of the membrane template, is likely to be the basis of the altered final materials morphology, resulting in the formation of nanoparticle chains. Such growth is similar to those observed for Pd NPNs generated inside of peptide assembled scaffolds previously,^{34, 36, 37} where a similar growth mechanism has been proposed.

Since the NP shape/morphology can significantly influence their catalytic performance, we used these Pd⁰ materials templated by the peptoid assemblies for the hydrogenation of two olefinic alcohols, allyl alcohol and 3-buten-2-ol (Figure 5a). Olefin hydrogenation reactions are routinely used for chemical synthesis, where the results of materials templated by peptoid assemblies can be directly compared with other Pd⁰ materials with similar structures. For these reactions, the Pd catalysts were dispersed in water and bubbled with H₂ prior to substrate addition. Aliquots were extracted over time to monitor product formation, from which turnover frequency (TOF) values were determined. Note that TOF calculations were determined based upon the total Pd in the reaction to allow for a direct comparison to appropriate comparable materials.^{30-32, 38} Figure 5b presents the TOFs for the membrane-templated Pd materials. For the allyl alcohol substrate (blue bars), a TOF of 1160 ± 331 mol product (mol Pd × h)⁻¹ was observed for the M-Pd50. No significant change in reactivity was observed for the M-Pd60 structures; however, increased catalytic reactivity was noted for the M-Pd70 and M-Pd80 materials with TOFs of 2610 ± 489 and 3465 ± 585 mol product (mol Pd × h)⁻¹, respectively.

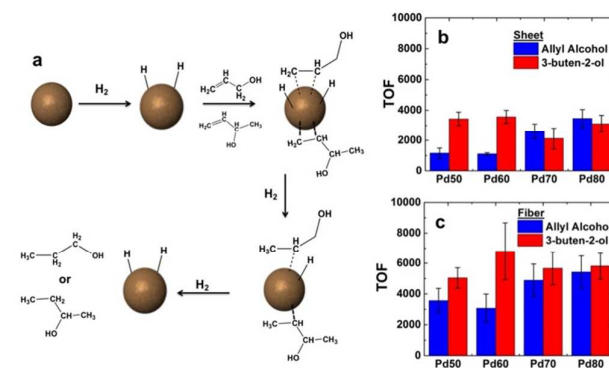


Figure 5. Catalytic analysis. (a) Scheme for Pd catalyzed olefin hydrogenation. TOFs for the hydrogenation of allyl alcohol (blue) and 3-buten-2-ol (red) for the (b) membrane- and (c) fiber-templated Pd⁰ materials.

When the same materials were employed for the hydrogenation of 3-buten-2-ol, changes in reactivity were evident (Figure 5b – red bars). In this regard, for the M-Pd50 and M-Pd60 materials, the TOF values dramatically increased to 3439 ± 442 and 3572 ± 423 mol product (mol Pd × h)⁻¹, respectively, which is nearly a three-fold enhancement in

reactivity. Interestingly, for the NPNs generated at the higher Pd loadings, no significant reactivity change was noted as compared to allyl alcohol with TOFs of 2125 ± 691 (M-Pd70) and 3118 ± 551 mol product (mol Pd \times h) $^{-1}$ (M-Pd80).

When the Pd⁰ nanoparticle chains templated by Pep_{Pd}-1 fibers were employed, enhanced reactivity was noted as compared to the Pd⁰ NPNs templated by peptoid membranes (Figure 5c). For allyl alcohol hydrogenation (blue bars) using F-Pd50, a TOF of 3569 ± 784 mol product (mol Pd \times h) $^{-1}$ was determined, which is a three-fold increase in reactivity compared to the membrane-derived materials. A similar increase in reactivity was observed for all of the fiber-templated materials where TOFs of 3072 ± 917 , 4886 ± 1053 , and 5423 ± 1057 mol product (mol Pd \times h) $^{-1}$ were observed for the F-Pd60, F-Pd70, and F-Pd80 materials, respectively. When the fiber-templated structures were used for the hydrogenation of 3-buten-2-ol (red bars), similar trends in increased reactivity were noted. In this respect, a greater TOF of 5038 ± 665 mol product (mol Pd \times h) $^{-1}$ was observed for the F-Pd50 materials. Upon increasing the metal loading to the F-Pd60, enhanced reactivity was quantified where the TOF was 6799 ± 1870 mol product (mol Pd \times h) $^{-1}$. A minimal change in reactivity was demonstrated for the F-Pd70 and F-Pd80 materials with TOFs of 5665 ± 1072 , and 5814 ± 844 mol product (mol Pd \times h) $^{-1}$, respectively.

The differences in reactivity as a function of the overall material structure are likely due to two effects: available reactive surface area and substrate structure/isomerization. When considering allyl alcohol hydrogenation employing the membrane-templated materials, increased reactivity was noted from the particles with a higher Pd loading. In these samples, a greater Pd surface area is anticipated due to their display on the membrane template. For the fiber-templated structures, higher reactivity was noted for all materials and substrates as compared to the same composition of inorganic materials generated using the membranes. This likely arises from a more efficient display of the Pd⁰ on the fiber due to the curved morphology of the biomimetic scaffold. This was evident by smaller degrees of NPN formation in the fiber-templated structures, leading to more diffused worm-like metallic materials in the sample for higher reactivity.

Substrate isomerization also plays an effect when comparing the reactivity of the primary and secondary olefinic alcohols,³¹ where TOF values decrease as substrate isomerization increases. This arises from a competition for the catalytic surface to drive the process (either isomerization or catalytic turnover). Increased isomerization is known for primary over secondary alcohols,³¹ thus giving rise to the generally higher TOFs for the 3-buten-2-ol substrate.

Relating the Pd⁰ nanomaterial catalysts templated by the peptoid assemblies to comparable structures previously reported, our materials demonstrated equivalent or increased reactivity. In this regard, Pd materials templated with the self-assembling R5 peptide have displayed TOF values of ~ 2900 and ~ 3400 mol product (mol Pd \times h) $^{-1}$ for allyl alcohol and 3-buten-2-ol hydrogenation, respectively.³² Crooks and co-workers have used dendrimer-encapsulated Pd NPs for allyl alcohol

hydrogenation, giving rise to a TOF of 220.0 mol product (mol Pd \times h) $^{-1}$.³⁸ Finally, Bruening and co-workers observed a TOF of up to 3500 mol product (mol Pd \times h) $^{-1}$ for Pd NPs embedded in polyelectrolyte films.³⁰ Comparing these studies with the peptoid-based systems, increased reactivity was observed for Pd⁰ NP chains templated by the Pep_{Pd}-1 fibers, while the Pd⁰ NPNs templated by the Pep_{Pd}-1 membranes demonstrated generally equivalent reactivity to previous systems. This further suggests that both the template and metal surface display are highly important to control reactivity and material properties.

Conclusions

In summary, these studies demonstrate that sequence-defined peptoids can be designed for tunable assembly of biomimetic materials that serve as unique templates to generate highly reactive Pd⁰ nanomaterials with variable morphologies. The morphology/orientation of the metallic components is controlled by the underlying morphology of peptoid assembly template, which has significant effects on the final material properties. This suggests that 3D organization of inorganic NPs is possible by using sequence-defined synthetic molecular systems that could be used for fine degrees of tuning their assembly morphology. Such capabilities could be readily adapted to different inorganic systems such as Au NPs for plasmonics, Fe₃O₄ NPs for magnetic materials, and CdS/ZnS quantum dots for optical/sensing applications. Since peptoids are easy to synthesize and exhibit protein-like side chain diversity, and various hierarchical structures can be assembled through controlling peptoid side-chain interactions and peptoid-surface interactions,^{15-23, 39} we expect that tunable peptoid assembly could offer a new platform acting as templates for controllable synthesis of inorganic nanomaterials with programmable structures and functions.

Conflicts of interest

There are no conflicts to declare.

Acknowledgements

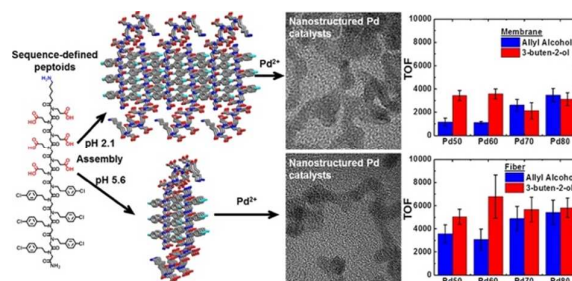
MRK and NAM acknowledge financial support from the University of Miami. XRD work was conducted at the Advanced Light Source with support from the Molecular Foundry, at Lawrence Berkeley National Laboratory, both of which are supported by the Office of Science, under Contract No. DE-AC02-05CH11231. Peptoid synthesis work was supported by the Materials Synthesis and Simulation Across Scales (MS³) Initiative through the LDRD fund at Pacific Northwest National Laboratory (PNNL). Peptoid self-assembly and characterization of peptoid membranes and fibers studies were supported by the US Department of Energy, Office of Science, Office of Basic Energy Sciences, Biomolecular Materials Program at PNNL. PNNL is multi-program national laboratory operated for

Department of Energy by Battelle under Contracts No. DE-AC05-76RLO1830.

Notes and references

1. M. Grzelczak, J. Vermant, E. M. Furst and L. M. Liz-Marzán, *ACS Nano*, 2010, **4**, 3591-3605.
2. C. L. Chen and N. L. Rosi, *Angew. Chem., Int. Ed.*, 2010, **49**, 1924-1942.
3. M. B. Dickerson, K. H. Sandhage and R. R. Naik, *Chem. Rev.*, 2008, **108**, 4935-4978.
4. M. Yang, H. Chan, G. Zhao, J. H. Bahng, P. Zhang, P. Král and N. A. Kotov, *Nat. Chem.*, 2016, **9**, 287.
5. M. A. Boles, M. Engel and D. V. Talapin, *Chem. Rev.*, 2016, **116**, 11220-11289.
6. A. Klinkova, R. M. Choueiri and E. Kumacheva, *Chem. Soc. Rev.*, 2014, **43**, 3976-3991.
7. X. Li and R. E. Schaak, *Angew. Chem., Int. Ed.*, 2017, **56**, 15550-15554.
8. J. L. Fenton, J. M. Hodges and R. E. Schaak, *Chem. Mater.*, 2017, **29**, 6168-6177.
9. M. J. Bradley, C. G. Read and R. E. Schaak, *J. Phys. Chem. C*, 2015, **119**, 8952-8959.
10. B. D. Briggs and M. R. Knecht, *J. Phys. Chem. Lett.*, 2012, **3**, 405-418.
11. T. R. Walsh and M. R. Knecht, *Chem. Rev.*, 2017, **117**, 12641-12704.
12. J. M. Slocik, F. Tam, N. J. Halas and R. R. Naik, *Nano Lett.*, 2007, **7**, 1054-1058.
13. J. M. Slocik, C. A. Crouse, J. E. Spowart and R. R. Naik, *Nano Lett.*, 2013, **13**, 2535-2540.
14. D. Mandal, A. Nasrolahi Shirazi and K. Parang, *Org. Biomol. Chem.*, 2014, **12**, 3544-3561.
15. J. Sun and R. N. Zuckermann, *ACS Nano*, 2013, **7**, 4715-4732.
16. H. Jin, Y.-H. Ding, M. Wang, Y. Song, Z. Liao, C. J. Newcomb, X. Wu, X.-Q. Tang, Z. Li, Y. Lin, F. Yan, T. Jian, P. Mu and C.-L. Chen, *Nat. Commun.*, 2018, **9**, 270.
17. X. Ma, S. Zhang, F. Jiao, C. J. Newcomb, Y. Zhang, A. Prakash, Z. Liao, M. D. Baer, C. J. Mundy, J. Pfaendtner, A. Noy, C.-L. Chen and J. J. De Yoreo, *Nat. Mater.*, 2017, **16**, 767-775.
18. H. Jin, F. Jiao, M. D. Daily, Y. Chen, F. Yan, Y.-H. Ding, X. Zhang, E. J. Robertson, M. D. Baer and C.-L. Chen, *Nat. Commun.*, 2016, DOI: 10.1038/ncomms12252, 12252.
19. F. Jiao, Y. Chen, H. Jin, P. He, C.-L. Chen and J. J. De Yoreo, *Adv. Funct. Mater.*, 2016, DOI: 10.1002/adfm.201602365, 8960-8967.
20. C. L. Chen, R. N. Zuckermann and J. J. DeYoreo, *ACS Nano*, 2016, **10**, 5314-5320.
21. J. Sun, X. Jiang, R. Lund, K. H. Downing, N. P. Balsara and R. N. Zuckermann, *PNAS*, 2016, **113**, 3954-3959.
22. E. J. Robertson, A. Battigelli, C. Proulx, R. V. Mannige, T. K. Haxton, L. S. Yun, S. Whitelam and R. N. Zuckermann, *Acc. Chem. Res.*, 2016, **49**, 379-389.
23. R. V. Mannige, T. K. Haxton, C. Proulx, E. J. Robertson, A. Battigelli, G. L. Butterfoss, R. N. Zuckermann and S. Whitelam, *Nature*, 2015, **526**, 415-420.
24. Y.-C. Chien, J. Tao, K. Saeki, A. F. Chin, J. L. Lau, C.-L. Chen, R. N. Zuckermann, S. J. Marshall, G. W. Marshall and J. J. De Yoreo, *ACS Biomaterials Science & Engineering*, 2017, **3**, 3469-3479.
25. C. L. Chen, J. H. Qi, J. H. Tao, R. N. Zuckermann and J. J. DeYoreo, *Sci. Rep.*, 2014, **4**, 6266.
26. C. L. Chen, J. H. Qi, R. N. Zuckermann and J. J. DeYoreo, *J. Am. Chem. Soc.*, 2011, **133**, 5214-5217.
27. F. Yan, L. Liu, T. R. Walsh, Y. Gong, P. Z. El-Khoury, Y. Zhang, Z. Zhu, J. J. De Yoreo, M. H. Engelhard, X. Zhang and C.-L. Chen, *Nat. Commun.*, 2018, **In press**, DOI: 10.1038/s41467-018-04789-2.
28. H. Heinz, B. L. Farmer, R. B. Pandey, J. M. Slocik, S. S. Patnaik, R. Pachter and R. R. Naik, *J. Am. Chem. Soc.*, 2009, **131**, 9704-9714.
29. R. N. Zuckermann, J. M. Kerr, S. B. H. Kent and W. H. Moos, *J. Am. Chem. Soc.*, 1992, **114**, 10646-10647.
30. S. Bhattacharjee and M. L. Bruening, *Langmuir*, 2008, **24**, 2916-2920.
31. D. B. Pacardo, E. Ardman and M. R. Knecht, *The Journal of Physical Chemistry C*, 2014, **118**, 2518-2527.
32. R. Bhandari, D. B. Pacardo, N. M. Bedford, R. R. Naik and M. R. Knecht, *The Journal of Physical Chemistry C*, 2013, **117**, 18053-18062.
33. J. A. Creighton and D. G. Eadon, *J. Chem. Soc. Faraday Trans.*, 1991, **87**, 3881-3891.
34. A. Jakhmola, R. Bhandari, D. B. Pacardo and M. R. Knecht, *J. Mater. Chem.*, 2010, **20**, 1522-1531.
35. A. Meister, S. Drescher, I. Mey, M. Wahab, G. Graf, V. M. Garamus, G. Hause, H.-J. Mögel, A. Janshoff, B. Dobner and A. Blume, *The Journal of Physical Chemistry B*, 2008, **112**, 4506-4511.
36. R. Bhandari and M. R. Knecht, *Langmuir*, 2012, **28**, 8110-8119.
37. R. Bhandari and M. R. Knecht, *Catalysis Science & Technology*, 2012, **2**, 1360-1366.
38. Y. Niu, L. K. Yeung and R. M. Crooks, *J. Am. Chem. Soc.*, 2001, **123**, 6840-6846.
39. A. S. Knight, E. Y. Zhou, M. B. Francis and R. N. Zuckermann, *Adv. Mater.*, 2015, **27**, 5665-5691.

For Table of Contents Use Only



Tunable peptoid assembly directs the control over structure and function of Pd nanomaterial catalysts.

ARTICLE

Journal Name